α2δ-2 is Required for Functional Postsynaptic Calcium Channel Nanodomain Signaling

Abbreviated Title: α2δ-2 organizes calcium signaling nanodomains

Kathleen A. Beeson[1,2], Gary L. Westbrook[3], Eric Schnell[2,4*]

1 Neuroscience Graduate Program, Oregon Health & Science University, Portland, OR, 97239; 2 Department of Anesthesiology and Perioperative Medicine, Oregon Health & Science University, Portland, OR, 97239; 3 The Vollum Institute, Oregon Health & Science University, Portland, OR, 97239; 4 Operative Care Division, Portland VA Health Care System, Portland, OR, 97239

*Corresponding Author

Eric Schnell, MD, PhD

schneler@ohsu.edu

3710 SW US Veterans Hospital Rd, P3ANES

Portland, OR 97239

Conflict of Interest Statement:

The authors declare no competing financial interests.

Acknowledgments:

This research was supported in part by the Department of Veterans Affairs, Veterans Health Administration, Office of Research and Development, Biomedical Laboratory Research and Development Merit Review Award I01-BX004938 (ES), a Department of Defense CDMRP Award W81XWH-18-1-0598 (ES), NIH T32NS007466 (KAB), NIH R01-NS080979 (GLW), and NINDS 1R21NS102948 (Ines Koerner/ES). We would like to acknowledge the OHSU Advanced Light Microscopy Center and imaging support from the NIH P30NS061800 (OHSU). The contents of this manuscript do not represent the views of the U.S. Department of Veterans Affairs or the United States Government.

Abstract

α2δ proteins (*CACNA2D1-4*) are required for normal neurological function, although the mechanisms whereby α2δ proteins control neuronal output remain unclear. Using whole-cell recordings of mouse cerebellar Purkinje cells, we show that α2δ-2 is required for coupling postsynaptic voltage-dependent calcium entry to effector mechanisms controlling depolarization-induced suppression of excitation as well as action potential afterhyperpolarization. Our findings indicate that α2δ-2 is necessary for the function of postsynaptic calcium signaling nanodomains.

Introduction

Many intracellular signaling cascades are triggered by a common messenger: calcium entering via voltage-gated Ca^{2+} channels (VGCCs) on the plasma membrane. Specificity of Ca^{2+}-dependent signaling at the membrane depends on proximity of VGCCs to effectors in functional "nanodomains," in which [Ca^{2+}] declines steeply with distance from a VGCC (1). These nanodomains are critical for neuronal function. For example, in Purkinje cells (PCs), depolarization-induced suppression of excitation (DSE) is initiated via Ca^{2+}-dependent endocannabinoid release that mediates short-term presynaptic depression (2-4). Likewise, VGCC-K_{Ca} clusters, expressed throughout PC somata and dendrites (5), generate the afterhyperpolarization (AHP) following action potentials, ultimately setting spontaneous spike rate (6, 7). Thus, molecules coupling VGCCs to effector-specific signaling critically contribute to transduction of neuronal outputs.

Auxiliary VGCC α2δ proteins (*CACNA2D1-4*) contribute to VGCC membrane trafficking in heterologous cells and neurons (8), and may play a role in presynaptic VGCC coupling to vesicle release machinery (9). However, little is known about auxiliary functions of α2δ outside of these contexts, and previous examination of their postsynaptic roles suggest Ca^{2+}-independent functions (10). Here we report that in PCs, which abundantly and exclusively express α2δ-2 (11-13), loss of α2δ-2 (*CACNA2D2*) disrupts two disparate forms of postsynaptic VGCC nanodomain signaling, demonstrating previously unappreciated roles for α2δ proteins in VGCC-effector coupling.

Results

At PC climbing fiber synapses, postsynaptic VGCC-mediated Ca^{2+} entry initiates retrograde endocannabinoid signaling, acutely reducing the probability of presynaptic vesicle release - a form of plasticity known as depolarization-induced suppression of excitation, or DSE (3, 4). Specificity of DSE signaling is achieved by tight functional coupling of postsynaptic VGCCs with Ca^{2+}-sensitive endocannabinoid release machinery (14). Using whole-cell recordings of PCs in acutely prepared brain slices from *CACNA2D2* KO and WT littermate mice, we investigated whether the absence of α2δ-2 affects this postsynaptic Ca^{2+}-dependent signaling.

We held PCs at -70 mV in voltage-clamp mode during climbing fiber axon stimulation and recorded evoked excitatory postsynaptic currents (EPSCs). In WT PCs, DSE elicited with a 250 ms depolarizing step reduced the amplitude of regularly evoked EPSCs by 25% (**Fig 1A-E**). In contrast, DSE was completely absent in KO PCs (**Fig 1B-E**). The *ducky* mouse, which also lacks α2δ-2 protein, has a reported ~30% decrease in PC somatic VGCC current density, which is thought to represent decreased surface trafficking (15). As the degree of climbing fiber DSE is related to the magnitude of Ca^{2+} influx, it is possible that the reduced VGCC density prevented DSE. Increasing the length of the depolarizing step enhances Ca^{2+} influx and DSE in wildtype mice (2); however, a four-fold increase in depolarizing step duration still failed to evoke DSE in α2δ-2 KO PCs **(Fig 1D-F**).

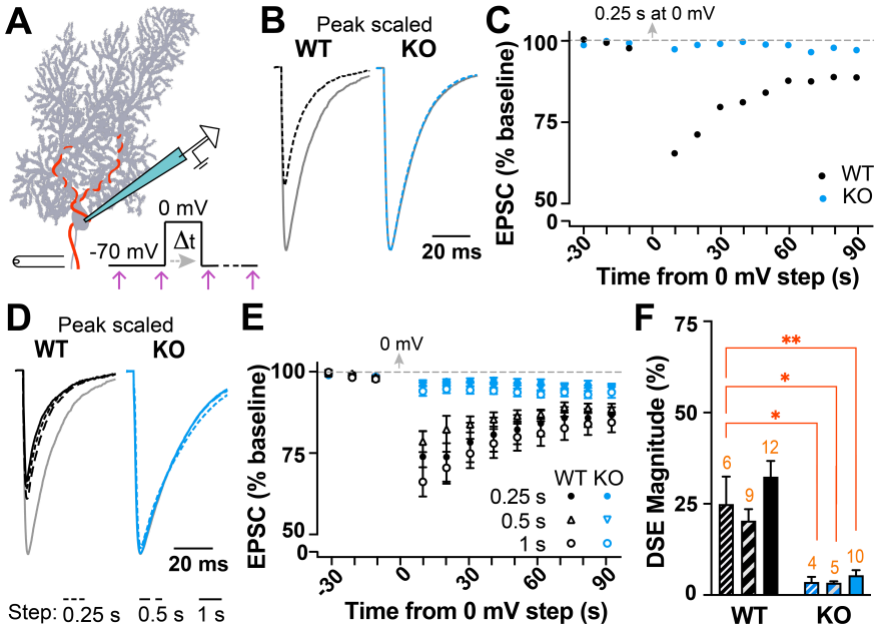

Figure 1 Depolarization-Induced Suppression of Excitation (DSE) reduces climbing fiber-EPSC amplitude in WT but not α2δ-2 KO Purkinje cells.

A) Schematic of whole-cell electrophysiological set-up. Purkinje cell (PC) is held at -70 mV using whole-cell voltage clamp while the innervating climbing fiber axon (red) is stimulated at 0.2 Hz (magenta arrows). After collection of baseline EPSCs, a depolarization step to 0 mV for a duration of 250 ms – 1s is delivered to the PC, and subsequent EPSCs are collected for >3 minutes.

B) Overlay of peak-scaled EPSC traces from WT (black) and KO (blue) PCs during baseline stimulation (gray) and 5 s post-depolarization step of 250 ms duration (dotted line).

C) EPSC amplitude timecourse from the representative experiment in B. Each point represents the average from two consecutive EPSCs at 0.2 Hz.

D) Overlay of peak-scaled EPSC traces from WT (black) and KO (blue) PCs during baseline (gray) and 5 s post-depolarization step of 250 ms (dotted line), 500 ms (dashed line), and 1 s (solid line) duration.

E) Summary of DSE timecourse from WT (black) and KO (blue) experiments using three different depolarization step durations: 250 ms (filled circle), 500 ms (triangle) and 1 s (open circle). Each point represents the average of two consecutive EPSCs at 0.2 Hz.

F) Magnitude of EPSC depression normalized to baseline in WT (black) and KO (blue) after 250 ms (fine stripe), 500 ms (wide stripe) and 1 s (solid) depolarization steps. n = cells (orange number over bars); each experiment

from > 3 mice. One-way ANOVA comparison to average WT 250 ms response, Dunnett's correction for multiple comparisons; * $p < 0.05$, ** $p < 0.01$, *** $p < 0.001$.

As DSE was not rescued by increasing activation of VGCCs in KO PCs, we hypothesized that functional coupling of Ca^{2+} influx to effector molecules was disrupted in the absence of α2δ-2. To examine this possibility, we lowered [EGTA] in our internal solution. As expected for WT PCs, decreasing [EGTA] from 10 mM to either 2 mM or 0.2 mM resulted in more profound DSE magnitude, which increased with longer voltage steps (**Fig 2A-C**), consistent with further diffusion of Ca^{2+} from its point of entry.

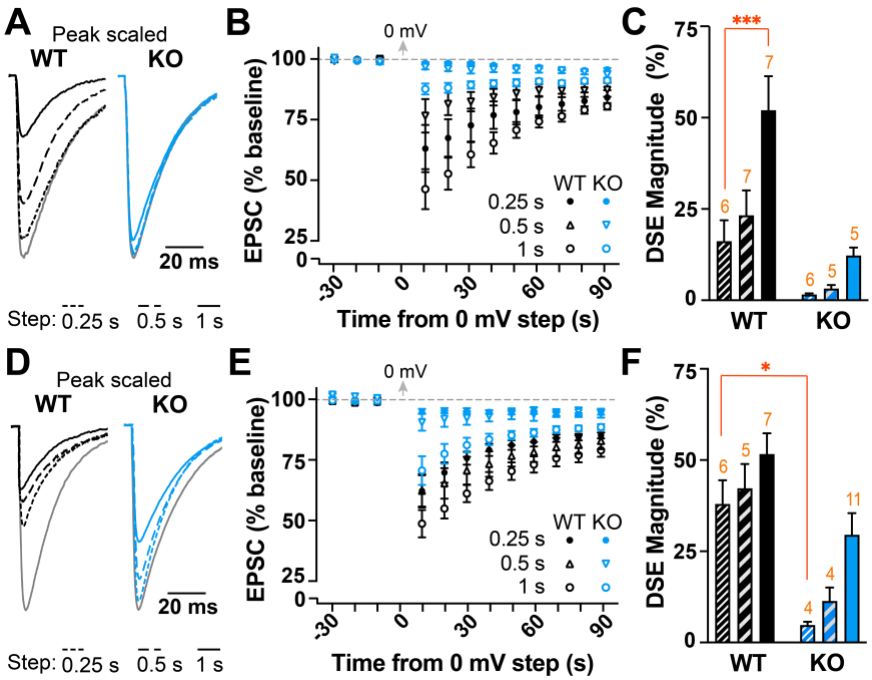

Figure 2 Reduced intracellular [EGTA] reveals climbing fiber DSE in the α2δ-2 KO.

A, D) Overlay of peak-scaled EPSC traces from WT (black) and KO (blue) PCs during baseline stimulation (gray) and 5 s post-depolarization step of 250 ms

(dotted line), 500 ms (dashed line), and 1 s (solid line) duration using intracellular solution containing 2 mM (**A**) or 0.2 mM (**D**) EGTA.

B, E) Summary of DSE timecourse from WT (black) and KO (blue) experiments using a 2 mM (**B**) or 0.2 mM (**E**) EGTA internal solution and three different depolarization step durations: 250 ms (filled circle), 500 ms (triangle) and 1 s (open circle). Each point represents the average of two consecutive EPSCs at 0.2 Hz.

C, F) Magnitude of EPSC depression normalized to baseline in WT (black) and KO (blue) after 250 ms (fine stripe), 500 ms (wide stripe) and 1 s (solid) depolarization steps using a 2 mM (**C**) or 0.2 mM (**F**) EGTA intracellular solution. n = cells (orange number over bars); each experiment from > 3 mice. One-way ANOVA comparison to average WT 250 ms response, Dunnett's correction for multiple comparisons; * $p < 0.05$, ** $p < 0.01$, *** $p < 0.001$.

More notably, however, reduced Ca^{2+} buffering restored DSE in KO PCs (**Fig 2D-F**), indicating that signaling mechanisms involved in DSE expression remained intact. As the reduced Ca^{2+} buffering primarily affects the distance of Ca^{2+} diffusion from its source, these data indicate that rather than affecting Ca^{2+} entry per se, α2δ-2 is necessary for tight functional coupling between VGCCs and endocannabinoid release.

To determine whether α2δ-2 affects coupling of other molecules to postsynaptic VGCC nanodomains, we focused on Ca^{2+}-dependent action potential AHPs. In PCs, the AHP is mediated by BK-type K_{Ca} channels (16, 17), and regulates sodium channel availability and PC firing rate (6, 18). To assess VGCC-K_{Ca} coupling, we recorded spontaneous spiking in PCs from WT and KO mice during whole-cell current-clamp recordings. In agreement with previous studies in the *ducky* mutant (15, 19), tonic spike rate in α2δ-2 KO PCs was reduced compared to WT (**Fig 3A-B**). More importantly, the AHP amplitude of individual spike waveforms was

107 consistently smaller in α2δ-2 KO cells (**Fig 3C-D**), indicating reduced K_{Ca} channel

108 activation (7, 16). Other membrane properties were unchanged in KO PCs, including

109 the resting membrane potential, maximum and minimum membrane polarization

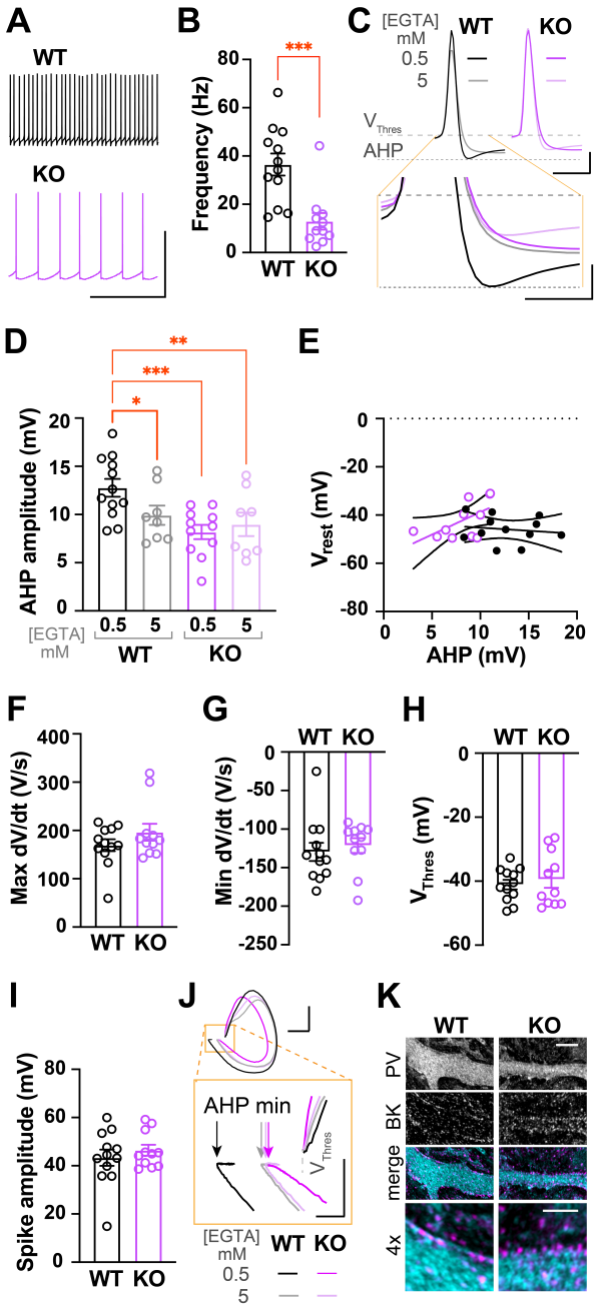

Figure 3 Spontaneous firing frequency, afterhyperpolarization (AHP) amplitude and Ca^{2+} coupling are reduced in the α2δ-2 KO.

A) Example traces of spontaneous action potentials in WT (black) and KO (magenta) PCs; scale = 50 mV, 0.5 s.

B) Summary of average spontaneous firing frequency in PCs. Student's unpaired t-test, $p < 0.0001$.

C) Average of 50 consecutive spontaneous action potentials from WT (0.5 mM EGTA, black; 5 mM EGTA gray) and KO (0.5 mM EGTA, magenta; 5 mM EGTA light purple) during tonic firing; scale = 10 mV, 2 ms. Gray dotted lines indicate V_{thres} as well as the minimum voltage during afterhyperpolarization (AHP). *Below*, enlarged overlay of traces to illustrate differences in V_{thres}-AHP amplitude; scale = 5 mV, 1 ms.

D) Summary of AHP amplitudes recorded after spontaneous action potentials using intracellular solution containing 0.5 mM EGTA or 5 mM EGTA. One-way

ANOVA comparison to average WT 0.5 mM EGTA response, uncorrected Fischer's LSD; * $p < 0.05$, ** $p < 0.01$, *** $p < 0.001$.

E) Correlation of AHP amplitude vs. resting membrane potential (V_m) in WT (black) and KO (magenta) PCs using 0.5 mM EGTA intracellular solution. Linear regression and 95% confidence interval; WT R^2 = <0.002; KO R^2 = 0.393.

F-I) Action potential waveform parameters in WT and KO PCs. No significant differences found for maximum dV/dt (**F**), minimum dV/dt (**G**), spike threshold (V_{thres}) (**H**) or spike height (**I**); unpaired Student's t-tests.

J) Phase plane plots of spontaneous spikes in WT (0.5 mM EGTA, black; 5 mM EGTA gray) and KO (0.5 mM EGTA, magenta; 5 mM EGTA light purple) PCs. Traces are aligned by threshold (V_{thresh}) for comparison; scale = 100 mV/ms, 20 mV. *Below*, enlarged inset to illustrate differences in AHP minimum amplitude between WT (arrows; 0.5 mM EGTA, black; 5 mM EGTA, gray) and KO (arrows; 0.5 mM EGTA, magenta; 5 mM EGTA, light purple); scale = 100 mV/ms, 5 mV.

K) Immunohistochemistry of WT and KO cerebellar slices stained for parvalbumin (PV; cyan) to indicate PC morphology, and the BK channel (magenta), which is involved in AHP generation; Scale 5 µm. *Below*, merged image at 4x zoom to illustrate membrane localization of BK channels; Scale 2 µm.

rates, spike threshold as well as spike height (**Fig 3E-J**), indicating that this effect was limited to the K_{Ca}-mediated AHP. Additionally, there was no change in BK membrane localization in PCs by immunohistochemistry (**Fig 3K**; Membrane BK density: WT = 0.82 ± 0.13, n = 4; KO = 0.75 ± 0.08, n = 3; p = 0.7; Student's unpaired t-test), consistent with normal BK expression and function found in other neurons in *ducky* mice (20).

To determine whether K_{Ca} channels were functionally uncoupled from VGCC-mediated Ca^{2+} influx in KO mice, we dialyzed PCs with an increased EGTA concentration (from 0.5 mM to 5 mM) sufficient to uncouple VGCC-BK signaling (21). This additional Ca^{2+} buffering reduced the AHP amplitude in WT cells to the

same amplitudes as the KO, and had no effect on the AHP in KO cells (**Fig 3C-D**). Thus, increased Ca^{2+} buffering uncoupled VGCC-K_{Ca} signaling in WT, but K_{Ca} channels were already functionally uncoupled in the α2δ-2 KO.

Discussion

As a primary signal in neurons, precise spatiotemporal regulation of Ca^{2+} influx is essential to maintain fidelity of Ca^{2+}-dependent processes. Consequently, the molecules controlling VGCC coupling to downstream effectors is critical to neuronal function. Since their initial discovery as VGCC-associated molecules, multiple lines of evidence suggest α2δ proteins are involved trafficking of VGCCs to the plasma membrane (8). However, these conclusions were necessarily based on heterologous expression systems, as most neurons express more than one α2δ isoform. Thus, information of postsynaptic auxiliary VGCC roles of α2δ proteins in neurons is limited. Because PCs selectively express only one isoform, α2δ-2 (11-13), the *CACNA2D2* KO mouse provides an ideal model to examine roles for α2δ-2 proteins in functional VGCC-signaling in postsynaptic compartments. Our results demonstrate that two distinct signaling mechanisms, DSE and K_{Ca} signaling, are disrupted in α2δ-2 KO PCs, indicating a functional loss of postsynaptic VGCC nanodomains (4, 5, 14, 21).

How does α2δ-2, a largely extracellular protein, mediate functional coupling of VGCCs with intracellular effector proteins? It is possible that α2δ-2 directly

142 associates with other extracellular proteins involved in VGCC domains (8). As
143 endocannabinoid machinery resides at synapses (22), and α2δ proteins are
144 important for synapse formation (10-13), α2δ could potentially regulate VGCC
145 nanodomains by binding to presynaptic adhesion proteins. Another possibility is
146 that α2δ-2 localizes VGCCs to lipid rafts. Though VGCCs are abundant in non-lipid
147 raft membrane fractions where they are independent of α2δ-2, VGCCs and α2δ-2
148 colocalize in lipid rafts isolated from cerebellar homogenates (23). Intriguingly, DAG
149 lipase-α, the enzyme responsible for synthesis of endocannabinoids involved in DSE,
150 has also been isolated in lipid rafts (24), and mislocalization of VGCCs away from
151 lipid rafts might explain the reduced basal endocannabinoid tone at cerebellar
152 synapses in the *ducky* mutant (25). Our results provide clues for future work to
153 directly assay α2δ-2 interacting proteins and subcellular localization of VGCCs in
154 PCs. The deficits in Ca^{2+}-dependent signaling we observed may contribute to the
155 dramatic neurologic phenotypes in α2δ-2 KO mice. Future investigations of the
156 coupling roles of other α2δ isoforms in neurons will provide valuable insights into
157 how these proteins impact neurological functions across the brain.

Materials & Methods

Animals: *Cacna2d2* knockout mice (*Cacna2d2*^{tm1Svi}, MGI = 3055290; generously supplied by Drs. Sergey Ivanov and Lino Tessarollo) were obtained as cryopreserved sperm and re-derived via *in vitro* fertilization on a C57BL/6J background. Breeding mice were kept heterozygous, and genotyping was performed as previously described (13). Mice were maintained in facilities fully accredited by the Association for Assessment and Accreditation of Laboratory Animal Care and veterinary care was provided by Oregon Health & Science University's Department of Comparative Medicine. All animal care and experiments were performed in accordance with state and federal guidelines, and all protocols were approved by the OHSU Institutional Animal Care and Use Committee.

Slice Preparation and Electrophysiology: Male and female mice were used between the ages of p21-30. KO and WT littermates were deeply anesthetized and transcardially perfused with ice-cold choline-based solution containing (mM): 125 choline-Cl, 2.5 KCl, 1.25 NaH_2PO_4, 0.44 ascorbate, 2 Na pyruvate, 3 3-myo-inositol, 10 D-glucose, 25 $NaHCO_3$, 7 $MgCl_2$, 0.5 $CaCl_2$ (osmolarity adjusted to 305 mOsm) and equilibrated with 95% O_2 and 5% CO_2 gas mixture. Acute 300 µm sagittal slices were cut from cerebellum using a vibratome (VT1200, Leica Microsystems), and incubated for 30 minutes in standard artificial cerebral spinal fluid (aCSF) at 34°C.

Voltage clamp recordings: Whole-cell recordings were obtained using 1-3 MΩ borosilicate glass pipettes filled with internal solution containing (in mM): 100

180 $CsMeSO_4$, 35 CsCl, 15 TEA-Cl, 1 $MgCl_2$, 15 HEPES, 2 ATP-Mg, 0.3 TrisGTP, 10
181 phosphocreatine, and 2 QX-314. A large batch of this internal base solution was
182 equally divided and 10, 2 or 0.2 mM EGTA was added to each third. All internals
183 were adjusted to pH 7.3 with CsOH and osmolarity to 293 mOsm. External solution
184 contained (in mM): 125 NaCl, 25 $NaHCO_3$, 1.25 NaH_2PO_4, 3 KCl, 25 Dextrose, 2 $CaCl_2$,
185 1 $MgCl_2$ (osmolarity adjusted to 300 mOsm) and was continuously perfused via
186 roller pump.

187 PCs were identified and recorded as previously described (13). Briefly, PCs
188 were chosen from the vermis lobe VI, were identified by soma size and location in
189 the PC layer, and whole-cell patch-clamp recordings were obtained in voltage clamp
190 mode. Cell capacitance, series resistance and input resistance monitored in real time
191 using intermittent -10 mV voltage steps. Inhibition was blocked in all experiments
192 by 10 µM SR95531 (Tocris), and 0.2-0.5 µM NBQX (Tocris) was included to maintain
193 voltage clamp of climbing fiber-mediated excitatory postsynaptic currents (EPSCs).
194 All voltage clamp recordings were performed at room temperature. Signals were
195 amplified with a MultiClamp 700B (Molecular Devices) amplifier and pipette
196 capacitance was compensated using MultiClamp software. Signals were low-pass
197 filtered at 6 kHz and sampled at 10 kHz, and digitized with a National Instruments
198 analog-to-digital board. All recordings were acquired and analyzed using IgorPro-
199 based (Wavemetrics) software.

200 For DSE experiments, PCs were held at -70 mV while climbing fiber-mediated
201 EPSCs were evoked using a monopolar glass electrode in the granule cell layer. After

obtaining 2 minutes of baseline responses at 0.2 Hz, a depolarizing voltage step to 0 mV of 1 s, 500 ms or 250 ms duration was delivered to induce DSE, after which PCs were returned to -70 mV and 0.2 Hz stimulation was continued. DSE plasticity is acute, and most synapses recover back to baseline EPSC amplitudes within < 60 seconds (2). As a small amount of "run down" was routinely observed in the evoked CF-mediated EPSC amplitude, DSE inclusion criteria required EPSC amplitudes to return to 80% baseline within 2 minutes post-stimulation (opposed to "stepping" to decreased amplitude without recovery). A minimum of 5 minutes were waited between DSE inductions, and step length was randomized throughout experiment. Series resistance was not compensated; cells with series resistance >10 MΩ, or a >2 MΩ change in series resistance over the course of the experiment were excluded.

For analysis, EPSC amplitudes were binned every 10 seconds (2 traces) and normalized to the 1 minute of baseline immediately preceding the depolarizing step. The 'DSE magnitude' (e.g. Figure 2E) is based on the average of EPSC amplitude 5 and 10 s after the depolarizing step. Example traces shown are from 5 s after the depolarizing step. A minimum of 3 mice per genotype were used for each manipulation, with no more than 2 cells/treatment coming from one mouse. For data presentation, EPSC traces were off-line box-filtered at 1 kHz in Igor64 software.

Current clamp recordings: For spontaneous spike experiments, internal solution contained (in mM): 120 KCH_3SO_3, 10 HEPES, 10 NaCl, 2 $MgCl_2$, 0.5 EGTA, 4 ATP-Mg, 0.3 Tris-GTP, and 14 phosphocreatine, pH 7.35 adjusted with KOH (osmolarity adjusted to 293 mOsm). A stock of EGTA solution was added to aliquots

of internal, to increase [EGTA] to 5mM as needed. Synaptic inhibition was achieved with 10 μM SR95531 (Tocris) and 10 μM NBQX (Tocris), and recordings were made at 36°C using an in-line heater. PCs in whole-cell mode from vermis lobe VI were first held in voltage clamp mode to monitor access series and input resistance before switching to current clamp. Changes in access were corrected with bridge balance using Multiclamp software. For increased action potential waveform resolution, some current clamp experiments were sampled at 50 kHz.

Spontaneous spikes from tonically firing PCs with < 400 pA holding current and < 10 MOhm series were analyzed using the Igor64 Neuromatic tools. Firing frequency data was collected from 10 seconds of recording, which yielded ~100-500 spikes. Action potential properties were assessed by averaging 50 consecutive spikes. Afterhyperpolarization (AHP) amplitude was measured as the difference between the threshold voltage (V_{thres} = depolarization rate >10 V/s) and the minimum voltage reached within 5 ms of spiking. All current clamp data was taken at least 3 minutes after break-in to allow time for internal solution to dialyze. Spike traces were box filtered for data visualization, and phase plane plots were made using Igor64.

<u>Immunohistochemistry:</u> Immunohistochemistry was performed as described (13). Briefly, p21 WT and KO mice were deeply anesthetized and transcardially perfused with ice-cold PBS followed by 4% paraformaldehyde (PFA)-PBS. Following decapitation, brains were removed and fixed overnight in 4% PFA-PBS, and stored

in PBS at 4°C. Sagittal cerebellar slices were made at 50 µm thickness using a vibratome, and slices containing vermis lobe VI were permeabilized for 1 hr with 0.4% Triton-PBS with 10% normal horse serum at RT. Slices were stained with goat anti-Parvalbumin (Swant #PVG-213; 1:1000) and mouse anti-BK (Neuromab #73-022; 1:500) overnight at 4°C. Corresponding fluorescently labeled secondaries (Invitrogen; 1:500) were applied after rinsing 3x in PBS, and slices were mounted on glass cover slips using Fluoromount G (Sigma-Aldrich).

BK membrane expression was imaged using 63x oil immersion lens on a LSM980 microscope with ZEN software. ~7 µm z-stack images of primary PC dendrites were acquired at 0.15 µm intervals using the PV channel at 4.5 x zoom with 680 x 680 pixel resolution. Airyscan images were processed using default settings in ZEN. Quantification of membrane localized BK puncta was done by a separate researcher, blinded to genotype, using the most transverse section of dendrite from each z-stack. For presentation, images were processed in Fiji/ImageJ, illustrating 0.45 µm maximum projections, and the panel was assembled using Adobe Photoshop.

Statistics: The data were tested for normality using Shapiro-Wilk test. Data from male and female mice were grouped. The difference in magnitude of DSE between the WT 250 ms depolarization step condition and other groups were compared using a one-way ANOVA with Dunnett's correction for multiple comparisons. For current clamp data, student's unpaired t-tests were used for spike frequency

268 comparison between WT and KO. In current clamp experiments using 5 mM EGTA,
269 only AHP amplitude was significantly different (all other measures not shown). For
270 this data, a one-way ANOVA with Fisher's LSD was used to compare all groups to
271 WT 0.5 mM condition. All electrophysiology experiments utilized at least 3 animals
272 per genotype, where n = # cells. For immunohistochemistry of BK membrane
273 density measurements, 2-4 images per animal were averaged (n = mice), and an
274 unpaired t-test was used for comparison. Data were graphed in Prism GraphPad
275 version 8 and are reported as the mean ± SEM. *$p<0.05$, **$p<0.01$, ***$p<0.001$.

References

1. Nakamura Y, Reva M, DiGregorio DA. Variations in Ca(2+) Influx Can Alter Chelator-Based Estimates of Ca(2+) Channel-Synaptic Vesicle Coupling Distance. J Neurosci. 2018;38(16):3971-87.

2. Brenowitz SD, Regehr WG. Calcium dependence of retrograde inhibition by endocannabinoids at synapses onto Purkinje cells. The Journal of Neuroscience. 2003;23(15):6373-84.

3. Brown SP, Safo PK, Regehr WG. Endocannabinoids inhibit transmission at granule cell to Purkinje cell synapses by modulating three types of presynaptic calcium channels. J Neurosci. 2004;24(24):5623-31.

4. Kreitzer AC, Regehr WG. Retrograde Inhibition of Presynaptic Calcium Influx by Endogenous Cannabinoids at Excitatory Synapses onto Purkinje Cells. Neuron. 2001;29:10.

5. Indriati DW, Kamasawa N, Matsui K, Meredith AL, Watanabe M, Shigemoto R. Quantitative localization of Cav2.1 (P/Q-type) voltage-dependent calcium channels in Purkinje cells: somatodendritic gradient and distinct somatic coclustering with calcium-activated potassium channels. J Neurosci. 2013;33(8):3668-78.

6. Raman IM, Bean BP. Ionic Currents Underlying Spontaneous Action Potentials in Isolated Cerebellar Purkinje Neurons. Journal of Neuroscience. 1999;19(5):12.

7. Womack MD, Chevez C, Khodakhah K. Calcium-activated potassium channels are selectively coupled to P/Q-type calcium channels in cerebellar Purkinje neurons. J Neurosci. 2004;24(40):8818-22.

8. Dolphin AC, Lee A. Presynaptic calcium channels: specialized control of synaptic neurotransmitter release. Nat Rev Neurosci. 2020;21(4):213-29.

9. Hoppa MB, Lana B, Margas W, Dolphin AC, Ryan TA. alpha2delta expression sets presynaptic calcium channel abundance and release probability. Nature. 2012;486(7401):122-5.

10. Eroglu C, Allen NJ, Susman MW, O'Rourke NA, Park CY, Ozkan E, et al. Gabapentin receptor alpha2delta-1 is a neuronal thrombospondin receptor responsible for excitatory CNS synaptogenesis. Cell. 2009;139(2):380-92.

11. Cole RL, Lechner SM, Williams ME, Prodanovich P, Bleicher L, Varney MA, et al. Differential distribution of voltage-gated calcium channel alpha-2 delta

(alpha2delta) subunit mRNA-containing cells in the rat central nervous system and the dorsal root ganglia. J Comp Neurol. 2005;491(3):246-69.

12. Lein ES, Hawrylycz MJ, Ao N, Ayres M, Bensinger A, Bernard A, et al. Genome-wide atlas of gene expression in the adult mouse brain. Nature. 2007;445(7124):168-76.

13. Beeson KA, Beeson R, Westbrook GL, Schnell E. alpha2delta-2 Protein Controls Structure and Function at the Cerebellar Climbing Fiber Synapse. J Neurosci. 2020;40(12):2403-15.

14. Brenowitz SD, Best AR, Regehr WG. Sustained elevation of dendritic calcium evokes widespread endocannabinoid release and suppression of synapses onto cerebellar Purkinje cells. J Neurosci. 2006;26(25):6841-50.

15. Donato R, Page KM, Koch D, Nieto-Rostro M, Foucault I, Davies A, et al. The ducky(2J) mutation in Cacna2d2 results in reduced spontaneous Purkinje cell activity and altered gene expression. J Neurosci. 2006;26(48):12576-86.

16. Edgerton JR, Reinhart PH. Distinct contributions of small and large conductance Ca2+-activated K+ channels to rat Purkinje neuron function. J Physiol. 2003;548(Pt 1):53-69.

17. Niday Z, Bean BP. BK channel regulation of after-potentials and burst firing in cerebellar Purkinje neurons. J Neurosci. 2021.

18. Womack M, Khodakhah K. Active Contribution of Dendrites to the Tonic and Trimodal Patterns of Activity in Cerebellar Purkinje Neurons. The Journal of Neuroscience. 2002;22(24):10603-12.

19. Walter JT, Alvina K, Womack MD, Chevez C, Khodakhah K. Decreases in the precision of Purkinje cell pacemaking cause cerebellar dysfunction and ataxia. Nat Neurosci. 2006;9(3):389-97.

20. Fell B, Eckrich S, Blum K, Eckrich T, Hecker D, Obermair GJ, et al. alpha2delta2 Controls the Function and Trans-Synaptic Coupling of Cav1.3 Channels in Mouse Inner Hair Cells and Is Essential for Normal Hearing. J Neurosci. 2016;36(43):11024-36.

21. Fakler B, Adelman JP. Control of K(Ca) channels by calcium nano/microdomains. Neuron. 2008;59(6):873-81.

22. Uchigashima M, Narushima M, Fukaya M, Katona I, Kano M, Watanabe M. Subcellular arrangement of molecules for 2-arachidonoyl-glycerol-mediated retrograde signaling and its physiological contribution to synaptic modulation in the striatum. J Neurosci. 2007;27(14):3663-76.

345 23. Davies A, Douglas L, Hendrich J, Wratten J, Tran Van Minh A, Foucault I, et al.
346 The calcium channel alpha2delta-2 subunit partitions with CaV2.1 into lipid rafts in
347 cerebellum: implications for localization and function. J Neurosci.
348 2006;26(34):8748-57.

349 24. Rimmerman N, Hughes HV, Bradshaw HB, Pazos MX, Mackie K, Prieto AL, et
350 al. Compartmentalization of endocannabinoids into lipid rafts in a dorsal root
351 ganglion cell line. Br J Pharmacol. 2008;153(2):380-9.

352 25. Wang X, Whalley BJ, Stephens GJ. The du(2J) mouse model of ataxia and
353 absence epilepsy has deficient cannabinoid CB(1) receptor-mediated signalling. J
354 Physiol. 2013;591(16):3919-33.

355